

# Experimental study of a high speed flow inside a dual research ducted rocket combustor using laser doppler velocimetry

by

C. Brossard<sup>(1)</sup>, P. Gicquel, M. Barat and A. Ristori

Office National d'Etudes et de Recherches Aérospatiales  
Chemin de la Hunière  
91761 Palaiseau Cédex  
France

<sup>(1)</sup>E-Mail: Christophe.Brossard@onera.fr

## ABSTRACT

As part of a research program initiated at Onera with the aim to improve methodology for ramjet combustion chamber design and tuning by using validated CFD codes, an experimental study of the high speed flow inside the duct section of a 3D research ducted rocket combustor was conducted.

A 2D Laser Doppler Velocimeter was used to deduce velocity profiles and turbulence characteristics in the horizontal and vertical mid-sections of the combustor duct. Based upon these data, the flow field structure, and in particular the recirculation zone in the dome region, was characterized. Comparison between the results obtained in non-reacting and reacting flow cases is discussed. Comparison between seeding particles velocities and soot particles velocities produced by the flame is also discussed here. An image sampled from one of the flame movies recorded using a high speed digital video camera (1,000 and 4,000 i/s) is briefly presented.

## INTRODUCTION

Validation studies of numerical tools used to calculate the flow structure in Solid Ducted Rocket (SDR) or Liquid Fueled Ramjet (LFRJ) motors have, to our knowledge, always been made for non-reacting or in 2D flow cases only (Stull et al., 1985, Liou et al., 1988, Liou and Hwang, Chuang et al., 1989, Chao et al., Wu et al., 1995). This suggests that an experimental study of both SDR and LFRJ combustors with 3D reacting flow cases would be worthwhile in order to validate numerical tools for a large range of ramjet operating conditions.

To this end, a research program was initiated at Onera with the aim to improve methodology for ramjet combustion chamber design and tuning by using validated CFD codes. A three-dimensional ramjet combustor geometry (combustor model) was specifically defined and built for investigations in hot flow conditions with operating conditions of the combustor (pressure, velocity, temperature) comparable to real motors ones. This combustor was designed in order to be used either as a SDR or a LFRJ motor.

In the first part of the research program, cold low speed flow studies were completed (Ristori et al., 1999). The second part of the research program is dedicated to hot non-reacting and reacting flow studies. This paper presents the results obtained in the experimental study of the high speed flow inside the duct section of the combustor for both non-reacting and reacting (kerosene) cases. Two-dimensional Laser-Doppler Velocimetry (LDV) was used in order to obtain the flow characteristics under realistic high altitude flight conditions.

The flow structure was characterized through profiles of the local mean velocities and turbulent correlations, measured at several axial locations along the length of the duct section.

## RESEARCH DUCTED ROCKET COMBUSTOR

The LFRJ combustor, shown in Fig. 1, consists of a main combustor with two lateral air inlets and a liquid fuel (kerosene) injection located into the head end of the combustor.

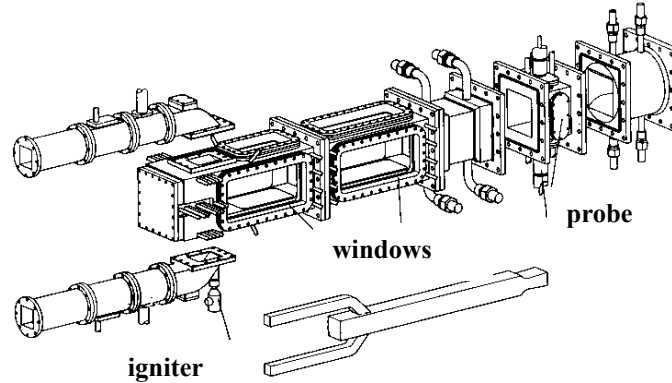


**Fig. 1. 3-D Schematic View of the Liquid Fueled Ramjet Combustor Model**

The ramjet combustion model, shown in Fig. 2 together with its key dimensions, is representative of a real engine. Its design characteristics are the following:

- The dome plate is flat and the dome height is adjustable from 30 mm to 100 mm; in this study, the dome depth was fixed to 50 mm;
- Combustor to air inlets area ratio = 2;
- Combustor Mach number = 0.35
- Exhaust Mach number = 1.55

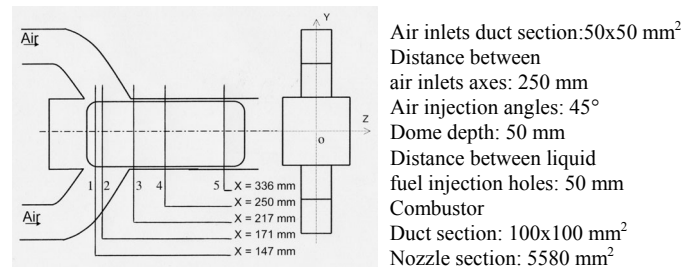


**Fig. 2. Schematic Side (left) and Back (right) Views of the Ramjet Combustion Model showing Key Dimensions**

Dimensions of the ramjet combustion model have been determined by using those engine characteristics as well as test rig performances. Optical access to the duct section of the combustor was provided by two fused silica windows, one located on each side of the combustor and represented in Figs. 1 and 2.

Test conditions for the high altitude flight case investigated in this study are given in table I in the reacting case for an equivalence ratio equal to 0.5.

**Table I. Test Conditions for the High Altitude Flight Case (Equivalence Ratio = 0.5)**

Inlet Air Total T° (K)	Air mass flow rate (kg/s)	Kerosene mass flow rate (kg/s)	Duct total pressure (MPa)	Duct total flame T° (K)
750	0.9	30	0.18	1650

**LASER DOPPLER VELOCIMETER SETUP**

A schematic view of the optical setup is shown in Fig. 3. A 15 W argon-ion laser source (Spectra 2040E) and a multicolor beam separator (Colorburst, TSI) were used to produce two laser beams at 514.5 nm and two laser beams at 488 nm wavelengths. The four beams were transmitted to the emitting optical head through four 25-m long monomode optical fibers with a 4-μm core diameter. The compact and light optical emitting head was built in order to form the optical probe volume from the four beams exiting the optical fibers (Labbé et al., 1991).

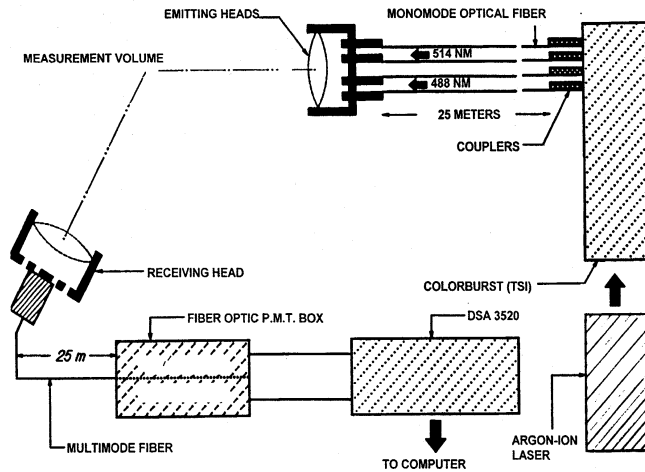


**Fig. 3. Schematic View of the 2-D Laser Doppler Velocimeter System**

For the receiving side, a commercial optical head (Aerometrics), connected to a 25-m long multimode optical fiber with a 160-μm core diameter, was used. Both emitting and receiving heads include a focus lens with a 500-mm focal length.

Since the duct section was equipped with a quartz window on each side of the combustor, the forward scattered light from the particles could be detected. A photograph of the combustor, showing in particular the two ram air inlets, the duct section equipped with quartz windows, and the LDV receiving head, is provided in Fig. 4. Doppler signals, amplified by photomultiplier tubes, were recorded and FFT-processed using the DSA (Doppler Signal Analyzer) software. For each measurement, statistical analysis was performed over a sample of 1,000 validated samples. The optical configuration allowed to measure the longitudinal component U (projection over the X-axis, represented in Fig. 2) and the vertical component V (projection over the Y-axis) of the particles velocity. Only the signals for which these two components of the velocity could be measured simultaneously (measurement in “coincidence”) were validated, the others were discarded. This procedure allowed to deduce the turbulent cross-correlation parameter from statistical analysis.

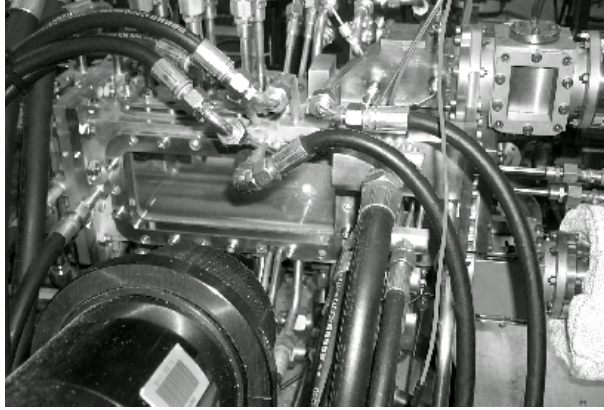


**Fig. 4: Photograph of the Combustor Showing the Duct Section Equipped with Quartz Windows and the LDV System.**

Both optical heads were installed on a 3D traverse system in order to measure velocity profiles over the volume of the duct corresponding to the windows size. In particular, profiles were measured along the vertical and horizontal mid-sections of the combustor for five different axial locations, indicated in Fig. 2. Also shown in Fig. 2 is the referential system ( $X, Y, Z$ ) used to present the velocity profiles results. The zero reference for the  $X$ -axis is located 80 mm upstream of the kerosene injection location, i.e. of the head end of the combustor. For both  $Y$  and  $Z$ -axes, the zero reference is located on the combustor axis.

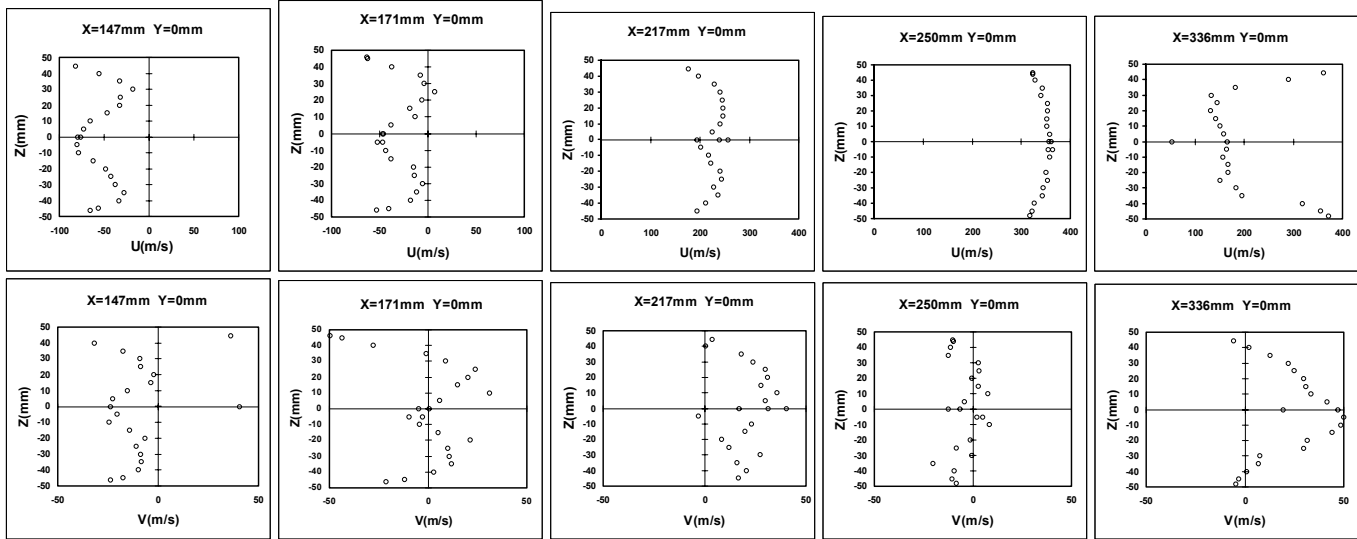
The seeding system consists of a pressurized cyclone generator for solid particles. This generator was developed and built specifically for this application. Both lateral ram air inlet flows were seeded in order to obtain a more uniform seeding of the flow in the duct section. The seeding particles were sampled from a mixture of magnesium oxide particles slightly diluted with nanometric Aerosil® (fumed silicon dioxide) particles, in order to fluidize the seeding particles mixture and reduce the risk for particles agglomeration.

## RESULTS AND DISCUSSION

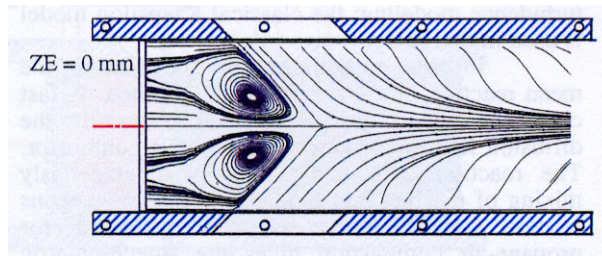
### Non-Reacting Flow

Figure 5 shows the profiles of the mean velocity components obtained in the horizontal mid-section of the combustor ( $Y=0$ ) for the five axial locations investigated in the non-reacting flow case. The air flow was preheated to an inlet total temperature of 750K. Upstream of the 171 mm axial location included, the longitudinal mean velocity  $U$  was negative. This reverse flow exhibited a local maximum of 80 m/s in velocity on the axis and two local minima at around  $Z=\pm 30$  mm, i.e. a location close to the outer edges location of the air inlet sections in the horizontal direction ( $Z=\pm 25$  mm). These results evidence the presence of a strong recirculation zone in the dome region, caused by the jet impingement of the two ram air streams and the existence of free volume at the head end of the combustor. This recirculation zone is represented in Fig. 6, which was obtained by Ristori et al. (1999) from computations performed for a similar combustor model. This combustor model was made of plexiglass and used for cold flow experiments; it was upscaled with a factor of 1.6 compared to the model investigated in the current study. Due to the symmetry of the combustor model with respect to its horizontal mid-section, there are two counter-rotating vortices in the dome region. The presence of these two vortices is evidenced by the velocity profiles components obtained in the vertical mid-section of the combustor ( $Z=0$ ) for the five same axial locations, and represented in Fig. 7. While the  $U$ -profiles in Fig. 5 are symmetric with respect to the  $Z=0$  vertical mid-section, the  $V$ -profiles in Fig. 7 are anti-symmetric with respect to the  $Y=0$  horizontal mid-section, due to the change in sign of the vertical component of the velocity.

In Fig. 7, the profiles obtained for  $X=147$  mm and  $X=171$  mm show that the value of  $U$  increased farther from the axis. The value of  $U$  became positive as the probe volume was moved away from the recirculation zone into the air inlet streams region. For an axial location  $X=171$  mm, the maximum velocity, obtained at  $Y=-40$  mm, was equal to 280 m/s for both  $U$  and  $V$  components. This corresponds to an orientation of the velocity vector of  $45^\circ$  and a velocity equal to 396 m/s, in agreement with the mean velocity of 345 m/s deduced from global measurements in the air inlets. It should be noted that in Fig. 5 none of the transverse horizontal profiles measured at  $Y=0$  for the vertical velocity component  $V$  is flat; however, flat profiles would be expected based upon the symmetry of the combustor model with respect to its horizontal mid-section. Based upon the negative values obtained for an axial location of  $X=147$  mm, this could be due to an actual location of the section  $Y=0$  slightly (the value of  $V$  never exceeds 50 m/s for all 5 axial locations investigated) above the horizontal mid-section.



**Fig. 5. Profiles of the Mean Longitudinal (U) and Vertical (V) Velocity Components Measured in the Horizontal Mid-Section of the Combustor (Non-Reacting Flow Case)**



**Fig. 6. Schematic of the Flow Pattern in the Combustor (Ristori et al., 1999) for  $Z=0$  mm (Non-Reacting Flow Case)**

The axial profiles of the mean velocity components in the duct section of the combustor obtained in the non-reacting flow case are represented in Fig. 8-a. The downstream limit of the recirculation zone in the dome region, as defined by the axial location for which  $U=0$ , was estimated to be  $X=184$  mm for the non-reacting flow case.

Figure 9 shows the transverse profiles of the turbulent fluctuations and cross-correlations deduced from the LDV measurements in the horizontal mid-section ( $Y=0$ ). In particular, for the axial location  $X=147$  mm, these profiles are shaped similarly to the profiles of the mean velocity components in Fig. 5. This indicates that the turbulence level is lower on the axis and stronger near the outer edges location of the air inlet sections in the transverse direction.

For an axial location of  $X=217$  mm, the transverse profiles in the horizontal and vertical mid-sections, represented in Fig. 5 and 7, respectively, show a local minimum in the longitudinal mean velocity  $U$  located on the combustor axis. At that point, the flow was still accelerating along the horizontal mid-section of the combustor, following the impingement of the two ram air streams. This acceleration continued up to at least  $X=250$  mm, where the longitudinal velocity reached 350 m/s on the axis. However, while the transverse profile in the horizontal mid-section of the combustor in Fig. 5 is rather flat at this axial location, the profile in Fig. 7 indicates a sharp decrease of the longitudinal velocity with the distance to the axis in the vertical direction. This shows a restriction of the flow near the horizontal mid-section of the combustor. Analysis of Figs. 5, 7, 8 and 9 reveals that a dramatic change occurred in the flow structure between the axial locations  $X=250$  mm and  $X=336$  mm. For  $X=336$  mm, the transverse longitudinal velocity profile in Fig. 7 became rather flat in the vertical direction, and associated with a significant decrease of the velocity level to approximately 60-80 m/s. On the contrary, the transverse profile in the horizontal direction in Fig. 5 shows the appearance of strong longitudinal velocity gradients in the horizontal mid-section of the combustor. On one hand, the velocity level along a distance equal

to half of the combustor width ( $|Z| < 25$  mm) around the combustor axis decreases from 350 m/s to 150 m/s between  $X=250$  mm and  $X=336$  mm, as also indicated by the axial profile in Fig. 8-a. On the other hand, the longitudinal velocity profile for  $X=336$  mm exhibited a sharp velocity increase in the side-walls region ( $|Z| > 25$  mm) from 150 m/s to 370 m/s. Therefore, the impingement of the two vertical ram air streams was followed by a deviation of the flow towards the side-walls. This change in the flow structure was associated with an increase in the turbulence level, as shown by the profiles in Fig. 9. In particular, the turbulent cross-correlation, which decreased to around zero between the head end of the combustor and the axial location  $X=250$  mm, significantly re-increased in level between  $X=250$  mm and  $X=336$  mm.

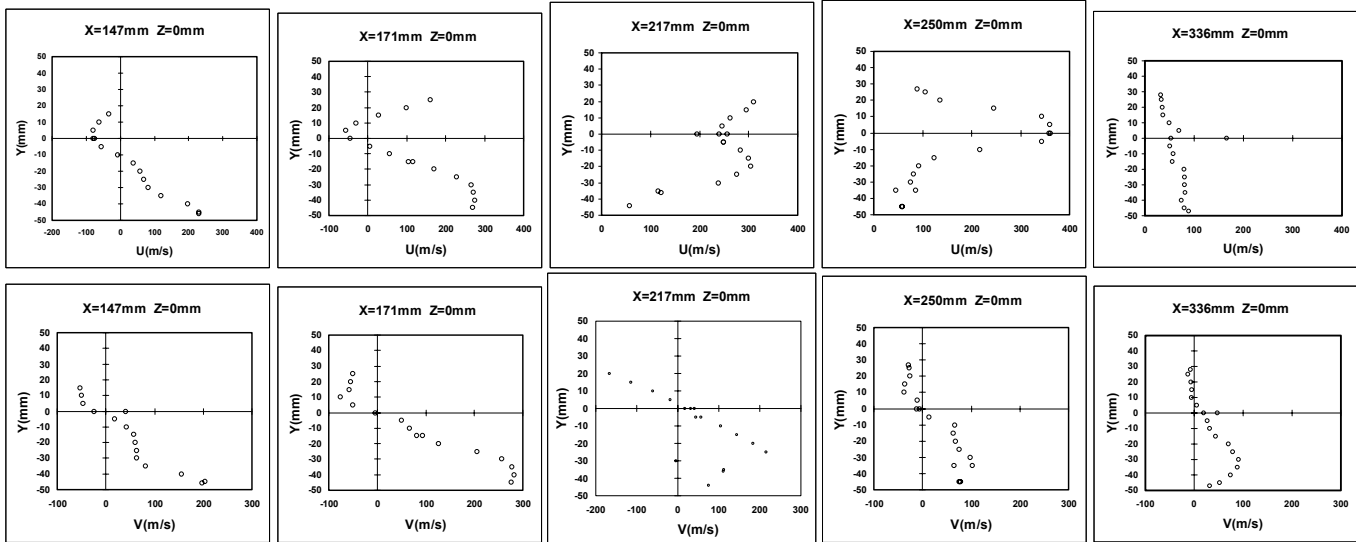


**Fig. 7. Profiles of the Mean Longitudinal (U) and Vertical (V) Velocity Components Measured in the Vertical Mid-Section of the Combustor (Non-Reacting Flow Case)**

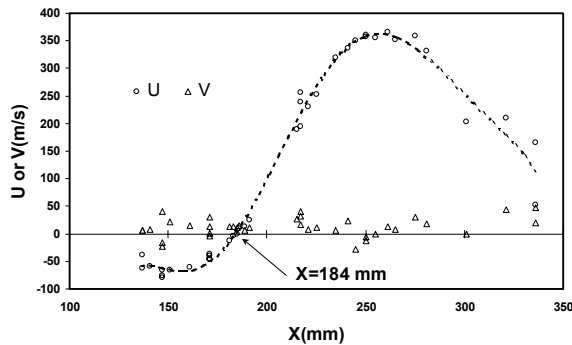


**Fig. 8-a. Non-Reacting Flow case**

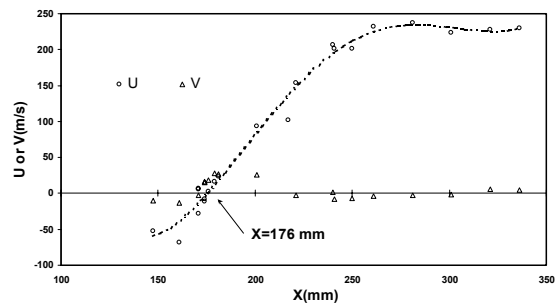


**Fig. 8-b. Reacting Flow case**

**Fig. 8. Axial Profiles of the Mean Longitudinal (U) and Vertical (V) Velocity Components**

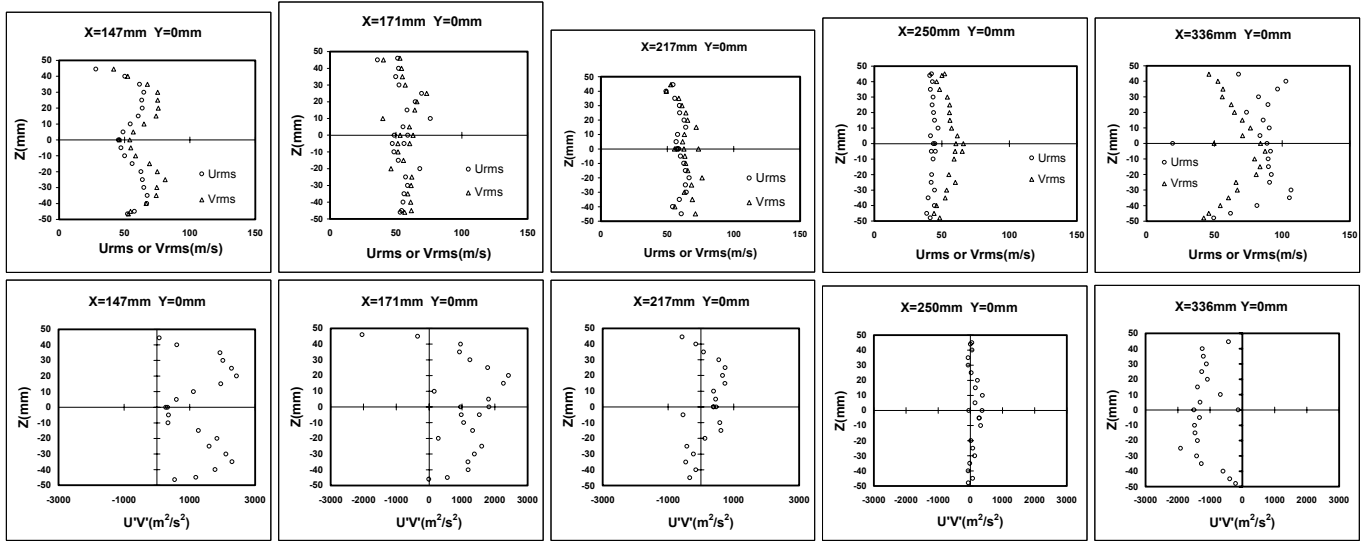


**Fig. 9. Profiles of the Turbulent Fluctuations and Cross-Correlations in the Horizontal Mid-Section of the Combustor (Non-Reacting Flow Case)**

### Reacting Flow

Figure 10 shows an instantaneous image of the turbulent flame inside the duct section, obtained from a high speed movie (1,000 i/s) recorded using a high speed digital video camera. Movies at higher speed (4,000 i/s) have also been recorded and are currently being analyzed to deduce some information about the unsteady characteristics of the flame, such as instability frequencies. Results of this work-in-progress will be discussed in future presentations. Figure 11 represents the transverse profiles of the mean velocity components obtained in the horizontal ( $Y=0$ ) and vertical ( $Z=0$ ) mid-sections of the combustor in the reacting flow case. For purpose of comparison, velocity profiles were measured both without and with flow seeding in order to obtain both the soot and magnesium oxide particles velocity profiles, respectively. The amount of scattering signals generated by the soot particles and validated during a given time interval was much lower than the total amount of signals detected during the same time in the presence of seeding particles. Therefore, the contribution of the soot particles to the histogram obtained in the presence of seeding particles could be neglected. Figure 11 shows that the profiles obtained are similar for both types of particles. The soot particles longitudinal velocities were lower than the seeding particles ones for  $X=250$  mm and  $X=336$  mm, with a difference which remained less than 60 m/s.

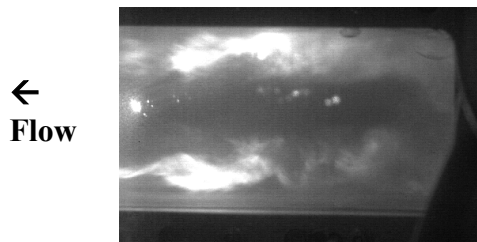


**Fig. 10. Instantaneous Image of the Flame**

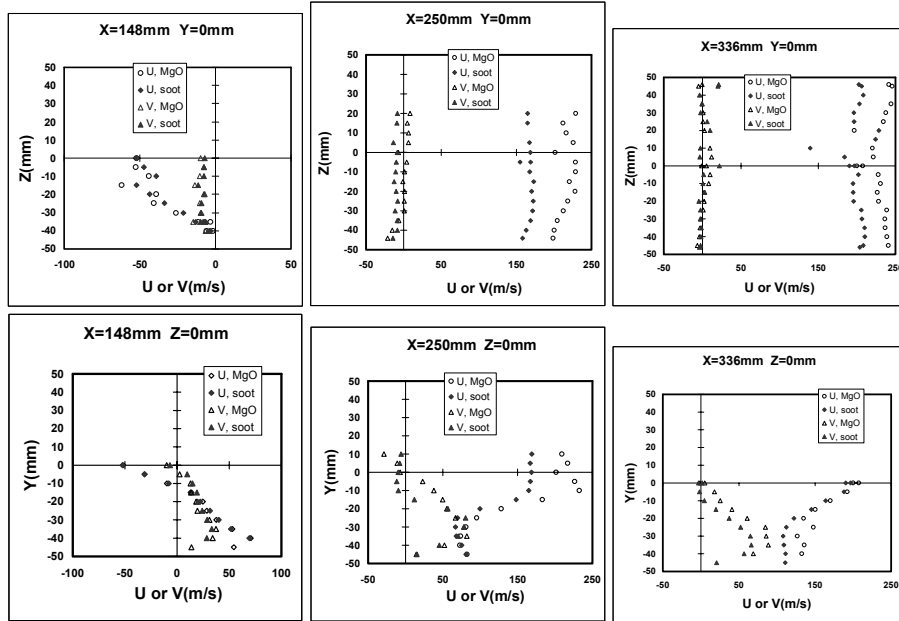


**Fig. 11 Profiles of the Mean Longitudinal (U) and Vertical (V) Velocity Components Measured in the Horizontal (Y=0) and Vertical (Z=0) Mid-Sections of the Combustor (Reacting Flow Case)**

Compared to the non-reacting flow case, the profiles in Fig. 11 show that no significant changes in the flow structure between X=250 mm and X=336 mm were observed in the reacting flow case. For X=250 mm, the profiles show that a restriction of the flow near the horizontal mid-section of the combustor exists, similarly to the non-reacting case, but with lower velocity gradients. For both cases, the longitudinal velocity near the bottom wall was around 70 m/s, but reached 350 m/s for the non-reacting flow case versus 230 m/s in the reacting flow case. Comparison of the longitudinal velocities obtained for X=250 mm with those obtained for X=336 mm shows that the profiles in both the vertical and horizontal directions tended to become more flat while keeping the same shape. In particular, for X=336 mm, in the horizontal mid-section of the combustor, the longitudinal velocity in the side-walls region was only slightly higher (250 m/s) than the longitudinal velocity in the axis (220 m/s). Therefore, the impingement of the two ram air streams did not result in a deviation of the flow towards the side-walls as in the non-reacting flow case. This difference between the two cases is also visible in Fig. 8, which shows that no decrease of the velocity was observed along the combustor axis downstream of X=250 mm axial location. This difference can be attributed to a much lower ram air velocity in the reacting flow case than in the non-reacting flow case due to the pressure increase caused by the combustion: the mean velocity in the ram air inlet ducts was 345 m/s in the non-reacting flow case versus only around 180 m/s in the reacting flow case. The axial profile in Fig. 8-b also indicates that the downstream limit of the recirculation zone in the reacting flow case was located more upstream (X=176 mm) than in the non-reacting case (X=184 mm).

## CONCLUSIONS

In this study, the high speed flow inside a dual research ducted rocket combustor, corresponding to a high altitude flight test condition, was investigated for both the non-reacting and reacting flow cases, using kerosene as the fuel. A 2D Laser Doppler Velocimeter was used to deduce velocity profiles and turbulence characteristics in the horizontal and vertical mid-sections of the combustor duct section.

The existence of a strong recirculation zone in the dome region with two large counter rotating vortices was evidenced by the results data. The downstream limit of this recirculation zone in the reacting flow case was located 8 mm upstream of the limit obtained for the non-reacting case.

Following the impingement of the two ram air streams, a significant deviation of the flow towards the side-walls of the combustor duct section occurred in the non-reacting flow case only.

The experimental results obtained in this study represent a significant data base, which will be utilized for comparisons with flow fields computations. This data base will be completed in the near future with additional data to be obtained for high speed flows corresponding to high and middle altitude flight conditions by using the PIV technique measurement.



## ACKNOWLEDGMENTS

The authors would like to thank the French Délégation Générale de l'Armement, Service des Programmes Nucléaires (DGA/SPNuc), for its financial support in this research program. Technical help provided by David Carru, Pascal Chérubini, and Jean-Jacques Lecout, as well as the contribution of Patrick Sainton to the data reduction and analysis, are gratefully acknowledged.

## REFERENCES

- Chao, Y.C., Chou, W.F. and Liu, S.S. (1995). "Computation of Turbulent Reacting Flow in a Solid-Propellant Ducted Rocket", *Journal of Propulsion and Power*, **11**, N°3.
- Chuang, C.L., Cherng, D.L., Hsieh, W.H., Settles, G.S. and Kuo, K.K. (1989). "Study of Flowfield Structure in a simulated Solid-Propellant Ducted Rocket Motor" 27<sup>th</sup> Aerospace Science Meeting, AIAA paper-89-0011.
- Labbé, J., Janssens, G. and Tanguy, B. (1991). "Design of a 3D Laser Doppler Velocimeter Fitted for Combustion Measurements, 4<sup>th</sup> International Conference on Laser Anemometry, Cleveland, OH.
- Liou, T.M., Hwang, Y.H. and Hung, Y.H. (1988). "Computational Study of Flow Field in Side Inlet Ramjet Combustors", 24<sup>th</sup> AIAA/ASME/SAE/ASEE Joint Propulsion Conference, AIAA paper-88-3010.
- Liou, T.M. and Hwang, Y.H. (1989). "Calculation of Flowfields in Side-Inlet Ramjet Combustors with an algebraic Reynolds Stress Model", *Journal of Propulsion and Power*, **5**, N° 6.
- Ristori, A., Heid, G., Cochet, A. and Lavergne, G. (1999). "Experimental and Numerical Study of the Turbulent Flow Inside a Dual Inlet Research Ducted Rocket Combustor", 14<sup>th</sup> Symposium ISOABE, Florence, Italy.
- Stull, F.D., Craig, R.R., Streby, G.D. and Vanka, S.P. (1985). "Investigation of a Dual Inlet Side Dump Combustor Using Liquid Fuel Injection" *Journal of Propulsion and Power*, **1**, N°1.
- Wu, P.K., Chen, M.H., Chen, T.H. (1995). "Flowfields in a Side-Inlet Ducted Ramrocket with/without Swirler", 31<sup>th</sup> AIAA/ASME/SAE/ASEE Joint Propulsion Conference and Exhibit, AIAA, Paper-95-2478.